Research Article Vol. 31, No. 25 / 4 Dec 2023 / Optics Express 42150
Optics EXPRESS

Elastoplastic contact model of pitch-based rough surface and its polishing characteristics

FUKUN LI,[1,2,3,4] YANG BAI,[1,2,3,4,*] HAIXIANG HU,[1,2,3,4] LONGXIANG LI,[1,2,3,4] LINGZHONG LI,[1,2,3,4] FENG ZHANG,[1,2,3,4] XIAO LUO,[1,2,3,4] AND XUEJUN ZHANG[1,2,3,4]

[1]*Changchun Institute of Optics, Fine Mechanics and Physics, Chinese Academy of Sciences, Changchun 130033, China*
[2]*University of Chinese Academy of Sciences, Beijing 100049, China*
[3]*State Key Laboratory of Applied Optics, Changchun, Jilin 130033, China*
[4]*Key Laboratory of Optical System Advanced Manufacturing Technology, Chinese Academy of Sciences, Changchun, Jilin 130033, China*
[*]*baiyang5406@sina.com*

Abstract: Fused silica glass is widely used in optical systems, including astronomical telescopes, laser systems, optical communications, and the semiconductor industry. At the same time, the surface quality of the fused silica directly determines the performance and precision of the system. In order to analyze the microscopic surface interaction based on the basis of tribology, a roughness contact model of pitch and fused silica glass surfaces was established. Analyze the performance parameters of contact materials, surface roughness, and the relationship between load and contact area. Pitch materials with a higher plasticity index have a larger elastoplastic contact area with the fused silica surface during the polishing process. The experimental results demonstrate that the surface quality of the polished fused silica improves as the plasticity index of the pitch material increases. At the same time, judging from the PSD curve results, the polished surface of the No. 55 pitch on the spatial-frequency band curve (10^0-10^1/mm) is significantly lower than the other two brands of pitch. Additionally, the Ra value of the workpiece surface roughness reaches 0.091 nm. The results of this study provide important theoretical guidance for achieving full-diameter, full-frequency ultra-smooth polishing of large-diameter complex curved surfaces.

© 2023 Optica Publishing Group under the terms of the Optica Open Access Publishing Agreement

1. Introduction

Fused silica is high-purity amorphous silicon dioxide (SiO_2) [1]. Compared with other types of glass, it has advantages such as high temperature resistance, corrosion resistance, high optical permeability, etc. Excellent physical and chemical properties [2]. Therefore, in ultra-precision optical systems, including X-ray, high-power laser, gravitational wave detection, and ultraviolet optical systems, fused silica glass usually plays a vital role in high-quality reflective or transmissive optical components. In these optical systems, the surface quality of optical components is considered to be the top priority, which directly determines the performance and precision of the optical system. The main indicators for evaluating optical surface properties include surface pattern, surface quality, surface roughness, etc. [3]. Fused silica has been researched and developed for various applications in military and defense, aerospace, semiconductors, and other fields [4,5]. However, the practical application of optically fused silica is still limited by its surface quality. For example, defects such as dust impurities, scratches, and corrosion pits on the surface of a laser lens Fused silica can easily cause irreversible damage because the accumulation of energy density at the defect exceeds the laser damage threshold [6]. Typically, silica materials are cut, ground, and polished prior to assembly and use. During this process, the polishing process directly determines the surface quality of the quartz part. However, the brittleness and

#506086 https://doi.org/10.1364/OE.506086
Journal © 2023 Received 22 Sep 2023; revised 10 Nov 2023; accepted 13 Nov 2023; published 29 Nov 2023

Optics EXPRESS

hardness of fused silica make it difficult to process. Traditional processing methods cannot achieve high precision. Microscopic cracks left on the surface will inevitably cause damage and fatigue to parts [7,8].

Computer controlled optical surface (CCOS) uses a computer-controlled polishing head to grind and polish optical components, which can effectively track the curvature changes of each point on the surface and precisely control the residence time, grinding pressure and polishing pressure of each point to achieve precise in recent years, it has received more and more attention [9]. In the CCOS process, the ideal processing effect is achieved by adjusting the polishing slurry, polishing parameters, and polishing grinding head material to eliminate defects and scratches. The schematic diagram of CCOS processing is shown in Fig. 1. The polishing grinding head is driven by a computer-controlled system. Under constant pressure, through the action of polishing abrasives, the fused silica glass is polished according to a certain trajectory, which includes the coordinated processes of chemical etching and mechanical removal.

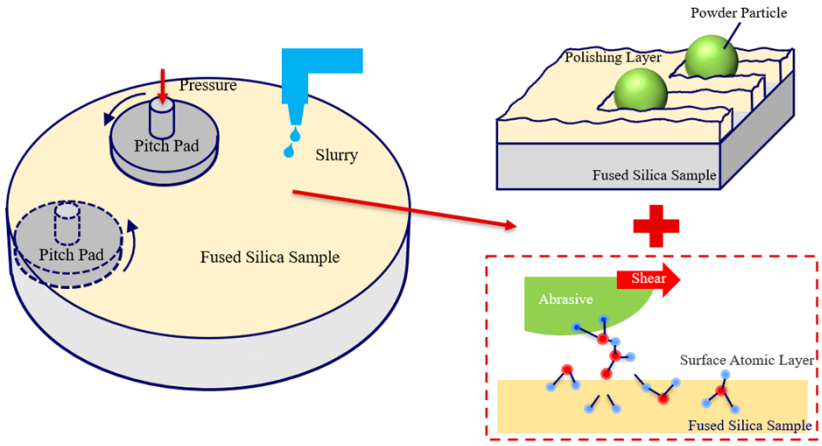

Fig. 1. Schematic diagram of CCOS processing.

Pitch is an important polishing tool, and the corresponding brand of pitch is typically selected based on processing requirements. However, during the actual processing, under the same processing conditions, the surface quality of different of pitch varies for different after processing. Most of the selection of pitch grades is based on traditional engineering experience, but the reasons for the differences between different grades of pitch have not been thoroughly explored. Based on the theory of tribology, this paper studies the influence of material properties, such as pitch hardness, elastic modulus, and surface roughness, on the outcomes of the processing. It also validates these findings through actual polishing experiments. This study has some constructive significance for full-diameter, full-frequency ultra-smooth polishing of large-diameter complex curved surfaces.

2. Theoretical analysis

2.1. Principle

Many researchers have studied contact with rough surfaces. The seminal contribution in this field was made by Greenwood and Williamson, who established the basic elastic contact model (GW model) [10]. In their model, the rough surface is represented by a group of hemispherical sharp corners with the same radius of curvature and a Gaussian distribution of height. Further assuming elastic (Hertzian) and independent microcontacts between the rough surface and the rigid smooth surface, the relationship between the true contact area and the total load as a function of the

Optics EXPRESS

distance between the plane and the average roughness is derived. By numerically comparing the GW model with other more general isotropic and anisotropic models, McCool believes that the GW model, although simple, can also give good results [11]. However, the GW model also has its limitations. it can only be used for contact problems with rough surfaces with a low plasticity index, where most of the bumps in contact are elastically deformed. Wazir Akbarz et al. used the improved GW model to properly model the contact mechanism between the wafer, slurry particles, and liner particles by considering the elastoplastic deformation during the contact process and proposed a coupled microcontact mechanics and slurry model of diffusion into wafers that predict the MRR in silica CMP [12]. Xia et al. established a microscale material removal model that combined the effects of applied load, material properties, ASD, and chemical reactions, used a three-system elastoplastic deformation and wet chemical etching to numerically predict the silicon surface topography, and explained the evolution of surface roughness and the origin of intrinsic polishing scratches at the nanoscale [13].

This paper proposes an elastoplastic rough contact model based on the rough surfaces of pitch and fused silica glass. The feature of this simulation is the representation of the transition state from elastic deformation to elastoplastic flow. Subsequent results of rough surface contact analysis showed that the elastoplastic contact of rough surfaces plays an important role in the macroscopic contact behavior of rough surfaces made of pitch and fused silica glass.

Since the surface of the workpiece to be polished is smoother compared to the pitch surface, the contact between two rough surfaces can be simplified by using an equivalent model of a single rough surface in contact with a smooth surface. Therefore, only the relationship between the rough surface and the rigid smooth plane is considered. The contact situation between the pitch surface and the fused silica surface is shown in Fig. 2.

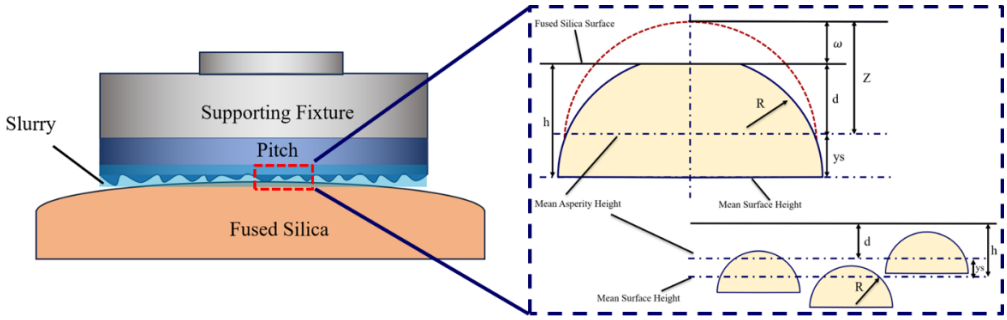

Fig. 2. Contact between pitch and fused silica surface.

2.2. *Rough surface contact model*

Consider the contact between the pitch surface and the fused silica surface, as shown in Fig. 2. Let z and d denote the height of the asperity and the average distance between the two surfaces, respectively. Then there is deformation ω:

$$\omega = z - d \tag{1}$$

According to the Hertzian contact theory [14], when a rough body undergoes elastic deformation, the elastic contact area A_e and contact pressure P_e of the spherical plane with radius R are:

$$A_e = \pi R\omega \tag{2}$$

$$P_e = \frac{4}{3}ER^{\frac{1}{2}}\omega^{\frac{3}{2}} \tag{3}$$

Optics EXPRESS

Critical deformation for elastic deformation:

$$\omega_e = \left(\frac{3\pi kH}{4E}\right)^2 R \tag{4}$$

In the formula, R is the radius of the asperity, and k is the surface average contact pressure coefficient, which is taken as 0.4 here. H is the hardness of the polished pitch material, while E is the equivalent elastic modulus.

$$E = \left(\frac{1-\mu_f^2}{E_f} + \frac{1-\mu_p^2}{E_p}\right)^{-1} \tag{5}$$

E_f and μ_f represent the elastic modulus and Poisson's ratio of fused silica glass, respectively, and E_p and μ_p represent the elastic modulus and Poisson's ratio of pitch, respectively. When $\omega<\omega_e$, the contact is elastic. When $\omega>\omega_e$, the contact is elastic-plastic or fully plastic.

When ω increases to ω_p, full plastic deformation occurs, and the average contact pressure at this time reaches H. Fully plastic contact area A_p[15]:

$$A_p = 2\pi R\omega \tag{6}$$

The corresponding contact pressure is:

$$P_p = 2\pi R\omega H \tag{7}$$

According to Zhao's research results [16], the critical contact deformation coefficient ω_p at the beginning of plastic deformation:

$$\omega_p \geq 54\omega_e \tag{8}$$

This expression indicates that the contact deformation at the onset of fully plastic deformation is at least 54 times that at initial yielding.

When the contact deformation ω is between ω_e and ω_p, that is, $\omega_e<\omega<\omega_p$, the asperity undergoes elastic-plastic deformation, because the total deformation at this stage is a mixture of elastic deformation and plastic deformation. According to the research results of Oh et al. [17], the elastic-plastic contact area is:

$$A_{ep} = \pi R\omega\left[1 - 2\left(\frac{\omega-\omega_e}{\omega_p-\omega_e}\right)^3 + 2\left(\frac{\omega-\omega_e}{\omega_p-\omega_e}\right)^2\right] \tag{9}$$

The contact pressure of the asperity in the elastic-plastic deformation state can be expressed as:

$$P_{ep} = \left[H - H(1-k)\frac{\ln\omega_p - \ln\omega}{\ln\omega_p - \ln\omega_e}\right] \times \pi R\omega\left[1 - 2\left(\frac{\omega-\omega_e}{\omega_p-\omega_e}\right)^3 + 2\left(\frac{\omega-\omega_e}{\omega_p-\omega_e}\right)^2\right] \tag{10}$$

The above theory for the contact of a rough surface with a rigid smooth surface can be used to model the elastoplastic contact between polished pitch and fused silica rough surfaces. If there are N asperities on a nominal area A_n, then the expected contact number of the asperities is:

$$n = N\int_d^\infty \Phi(z)dz = \eta A_n \int_d^\infty \Phi(z)dz \tag{11}$$

In the formula, η is the area density of asperity on the rough surface, and its value is taken as $5\times10^{10}\,\mathrm{m}^{-2}$, and $\Phi(z)$ is the probability density of the distribution of asperity height. The total

Optics EXPRESS

actual area A_t and load P_t of the contact between the two surfaces is the sum of the contributions of each asperity protrusion to all microcontacts.

For a given surface roughness distribution, the actual total contact area is A_t:

$$A_t(d) = A_{et}(d) + A_{ept}(d) + A_{pt}(d) \tag{12}$$

Total load P_t:

$$P_t(d) = P_{et}(d) + P_{ept}(d) + P_{pt}(d) \tag{13}$$

The meaning of the subscript t indicates the overall meaning. According to the above analysis results, the above two expressions were divided by A_n and A_nE for normalization. Further, all the length parameters and variables in the equation are normalized by σ, and the dimensionless equation of actual contact area A_t and load P_t is given by the following formula:

$$\begin{aligned} A_t^N &= \pi\beta \int_{h^N-y_s^N}^{h^N-y_s^N+\omega_e^N} \omega^N \Phi^N(z^N) dz^N \\ &+\pi\beta \int_{h^N-y_s^N+\omega_e^N}^{h^N-y_s^N+\omega_p^N} \left[1 - 2\left(\frac{\omega^N-\omega_e^N}{\omega_p^N-\omega_e^N}\right)^3 + 2\left(\frac{\omega^N-\omega_e^N}{\omega_p^N-\omega_e^N}\right)^2\right] \omega^N \Phi^N(z^N) dz^N \\ &+2\pi\beta \int_{h^N-y_s^N+\omega_p^N}^{\infty} \omega^N \Phi^N(z^N) dz^N \end{aligned} \tag{14}$$

$$\begin{aligned} P_t^N &= \frac{4}{3}\beta\left(\frac{\sigma}{R}\right)^{\frac{1}{2}} \int_{h^N-y_s^N}^{h^N-y_s^N+\omega_e^N} (\omega^N)^{\frac{3}{2}} \Phi^N(z^N) dz^N \\ &+\frac{\pi H\beta}{E} \int_{h^N-y_s^N+\omega_e^N}^{h^N-y_s^N+\omega_p^N} \left[1 - (1-k)\frac{\ln\omega_p^N - \ln\omega^N}{\ln\omega_p^N - \ln\omega_e^N}\right] \left[1 - 2\left(\frac{\omega^N-\omega_e^N}{\omega_p^N-\omega_e^N}\right)^3 + 2\left(\frac{\omega^N-\omega_e^N}{\omega_p^N-\omega_e^N}\right)^2\right] \\ &\times\omega^N \Phi^N(z^N) dz^N + \frac{2\pi H\beta}{E} \int_{h^N-y_s^N+\omega_p^N}^{\infty} \omega^N \Phi^N(z^N) dz^N \end{aligned} \tag{15}$$

In the formula,

$$\beta = \eta\sigma R \tag{16}$$

$$\omega^N = z^N - h^N + y_s^N \tag{17}$$

$$\Phi^N(z^N) = \frac{1}{\sqrt{2\pi}}\left(\frac{\sigma}{R}\right)^{\frac{1}{2}} e^{-\frac{1}{2}\left(\frac{\sigma}{\sigma_s}\right)^2 (z^N)^2} \tag{18}$$

β is the surface contact factor, which is related to the density of the surface asperity, the standard deviation of the surface height and the radius of the asperity. σ is the standard deviation of the surface height. In the above expressions, the ones marked with N in the upper corner are all normalized variables.

The relationship between h and σ of the surface micro-geometric model and d and σ_s of the roughness-based model is as follows [18]:

$$\sigma^2 = \sigma_s^2 + \frac{3.717 \times 10^{-4}}{\eta^2 R^2} \tag{19}$$

$$h = d + y_s \tag{20}$$

According to the above formula, the plasticity index ψ can be obtained:

$$\psi = \frac{2E}{\pi KH}\left(\frac{\sigma}{R}\right)^{\frac{1}{2}} \left(1 - \frac{3.717 \times 10^{-4}}{\eta^2 R^2 \sigma^2}\right)^{\frac{1}{4}} \tag{21}$$

In the formula, K is the maximum contact pressure factor, in this model, $K = 0.6$, σ_s is the standard deviation of the asperity height. It can be seen from the above formula that the plasticity index depends not only on the material properties but also on the surface morphology. Rough and soft surfaces have a higher plasticity index.

Optics EXPRESS

2.3. Theoretical analysis results

According to the model mentioned above, the contact behavior between two nominal planes of pitch and fused silica glass is studied within the range of contact load and plasticity index. The parameters of pitch and fused silica glass to be analyzed are shown in Table 1. Three commonly used polished pitches, Gugolz No. 55, No. 64, and No. 73 (Meller Optics Inc., Providence, USA), were selected. The performance parameters of the three types of pitch and fused silica glass can be found in relevant literature [19–21]. The σ/R and β values of different types of pitch are given in Table 2. The roughness and asperity height of the pitch surface were measured by a laser confocal microscope (LEXT OLS4100, Olympus, Tokyo, Japan), and the measurement results were averaged across four groups.

Table 1. Performance parameters of each material

Materials	Hardness (Pa)	Poisson's ratio	Elastic Modulus (GPa)
Gugolz 55	3.92×10^{8}	0.19	0.19
Gugolz 64	7.742×10^{8}	0.2	0.23
Gugolz 73	8.036×10^{8}	0.2	0.24
Fused Silica	1.05×10^{10}	0.17	74

Table 2. Pitch surface morphology parameters and plasticity index

Pitch	σ/R	β	ψ
Gugolz 55	1.475	0.0295	0.667
Gugolz 64	1.025	0.0205	0.232
Gugolz 73	0.790	0.0158	0.207

It can be seen from Fig. 3 that the ratio A_{ept}/A_t between the elastoplastic contact area and the actual contact area of the pitch and fused silica is a function of the pitch plasticity index ψ and the contact load P_t/A_nE, and the area ratio varies with the contact load and the plasticity index increases with the increase. It can be observed from the figure that at low loads, the deformation of the asperities is primarily elastic, but it transitions to elastoplastic deformation within a small range at high loads. In the case of a low plasticity index, the deformation is mainly elastic.

Figure 4 shows the relationship between the real contact area ratio A_t/A_n of pitch and fused silica glass, the dimensionless load P_t/A_nE and the plasticity index ψ of pitch. It can be seen that the ratio of the actual contact area to the total contact area increases as the load increases. However, for the pitch materials with three different plasticity indices, the ratios are very close.

Figure 5 shows the variation of dimensionless h/σ with P_t/A_nE under different plasticity exponents ψ. It can be seen that, at a given load, the separation between contacting rough surfaces increases as the plasticity exponent ψ of the pitch increases. For very smooth pitch surfaces or hard pitch materials (low ψ), the contact is mostly elastic. At low loads, the contact between the pitch and the fused silica glass surface is predominantly elastic. As the pitch surface becomes rougher or the pitch material becomes softer, there is increased plastic contact with the fused silica glass surface.

From the above analysis, it can be seen that under the same pressure, the total actual contact areas between the three types of polished pitch and the optical element surface are similar. However, the real difference lies in the elastic-plastic contact area and the average surface separation amount. Therefore, during the actual polishing process, the elastic-plastic contact characteristics between the polishing pitch and the surface of the optical element are important factors that affect the polishing results. Pitches with varying plasticity indexes have different elastic-plastic contact areas and average surface separation amounts. The following sections

Optics EXPRESS

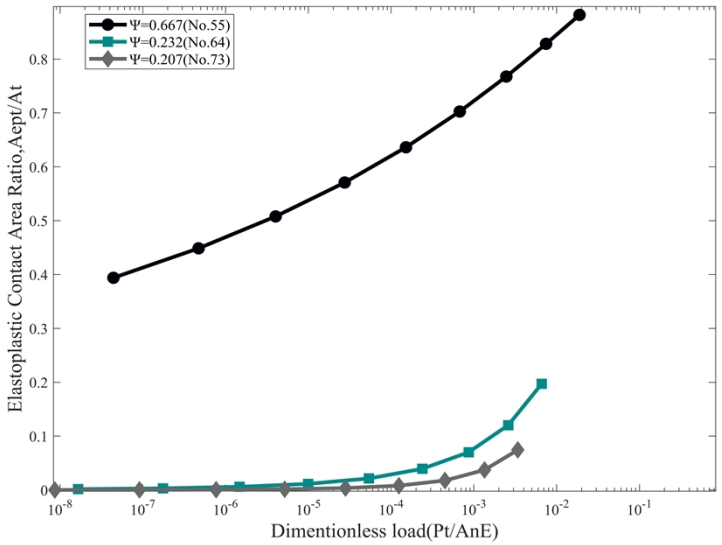

Fig. 3. The relationship between elastic-plastic contact and real contact area ratio A_{ept}/A_t, dimensionless load P_t/A_nE and plastic exponent ψ.

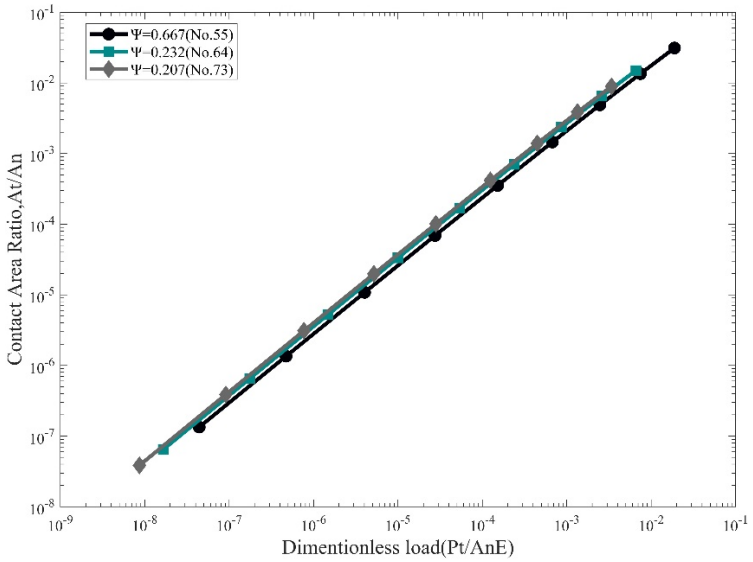

Fig. 4. Relationship between real contact area ratio A_t/A_n, dimensionless load P_t/A_nE and plastic exponent ψ.

Optics EXPRESS

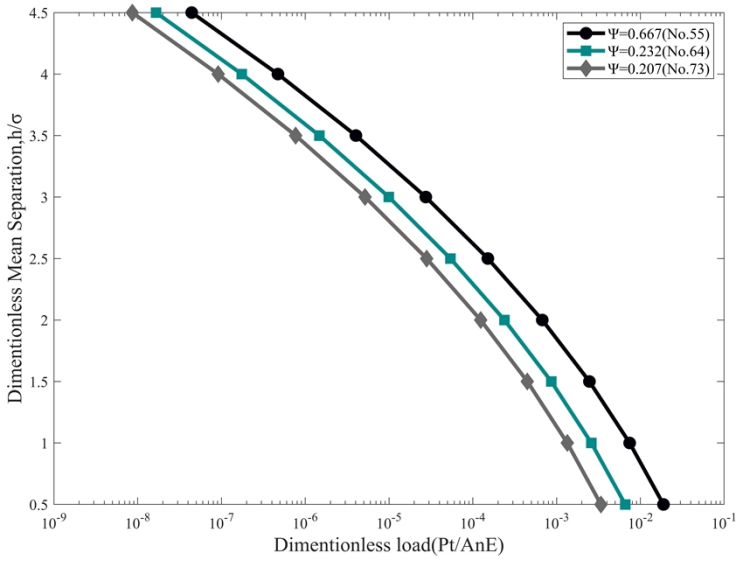

Fig. 5. Variation of dimensionless h/σ with P_t/A_nE under different plastic exponents ψ.

will examine the polishing characteristics of pitches with varying plasticity indexes through experiments. The corresponding relationship between different plasticity indexes and polishing results is then obtained.

3. Experiment

The processing and testing process of CCOS equipment is shown in Fig. 6. The polishing grinding head is driven by a robot (IRB 2600, ABB, Zurich, Switzerland) to perform the polishing process along a certain trajectory, as shown in Fig. 6(a). The polishing grinding head adopts the polishing pitch of Global Optics, and the base of the grinding head matched with the pitch is made of stainless steel. The grades of the polished pitch were used for experimental verification No. 55, No. 64, and No. 73 (Universal Photonics Inc., CP, Central Islip, NY, USA). Before starting the polishing process, it is recommended to make cross marks on the pitch surface to reduce the accumulation of abrasives during the polishing process, allowing the polishing abrasives can fully circulate more effectively at the polishing interface. The polishing slurry is 50 nm high-purity cerium oxide abrasive (Universal Photonics Inc., Central Islip, NY, USA). After the abrasive is mixed with deionized water at a concentration of 1:10, it is used after being fully shaken with a magnetic stirrer. Polishing experiments all use the new proportion of polishing slurry. The surface roughness of the polished fused silica glass was characterized by a white light interferometer (New View 9000, ZYGO, Connecticut, USA), as shown in Fig. 6(b).

Three pieces of fused silica glass (Shanghai Sikoty Optic & Electron Co., JGS2) with a diameter of 150 mm and a thickness of 15 mm were used as experimental workpieces for processing. The initial roughness results of the three pieces of fused silica glass are shown in Fig. 7. The surface roughness data of fused silica are all measured by a white light interferometer, and the average value of six groups of measurement data is taken. The lens magnification is 10 times, and the sampling area is 0.868mm × 0.868 mm. It can be seen that the initial roughness RMS values of the three pieces of fused silica are very close, which helps to reduce the experimental errors and ensure the accuracy of the subsequent polishing experimental results.

Optics EXPRESS

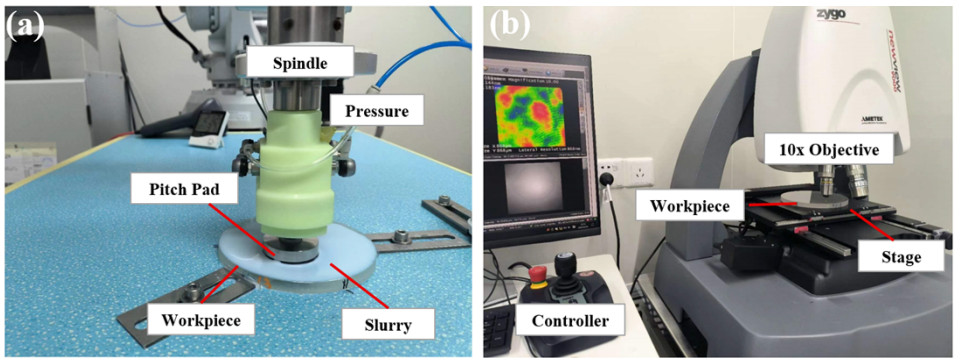

Fig. 6. Processing and testing device. (a) CCOS processing process; (b) testing process.

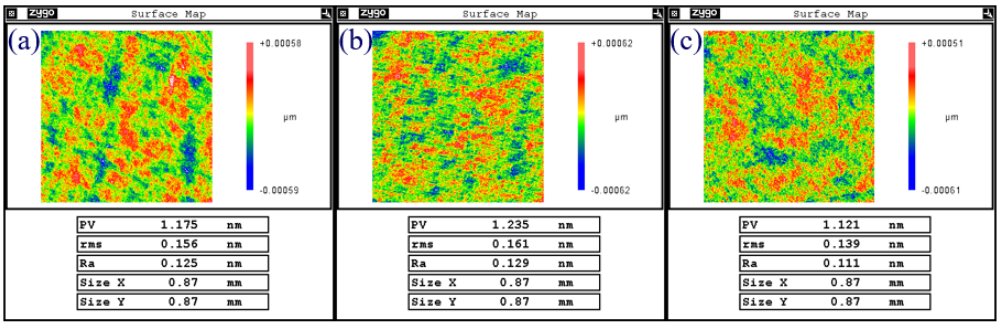

Fig. 7. Initial surface roughness of fused silica. (a) Surface roughness of No. 55 pitch before polishing; (b) Surface roughness of No. 64 pitch before polishing; (c) Surface roughness of No. 73 pitch before polishing.

Three grades of pitch polishing experiments were designed. The main parameters of the processing process are shown in Table 3. During the experiments, we will strictly control the relevant parameters listed in the table.

Table 3. Main parameters in the polishing process

Diameter(mm)	Speed (RPM)	Pressure (MPa)	Time(min)	Temperature (°C)
50	50	0.04	60	22±0.5

The processing trajectory adopts the commonly used Ross trajectory, and the eccentricity of the polishing grinding head is adjusted to 10 mm. Preheat the polishing grinding head for 30 seconds before each processing to ensure a better fit with the mirror surface. The pressure is kept constant during the polishing process, and the surface of the fused silica is cleaned with deionized water before processing to avoid the influence of impurities. Except for the different types of polishing pitch, all other polishing parameters and types of polishing fluids were consistent among the samples. After polishing, all samples were sequentially cleaned with deionized water and alcohol for subsequent experimental characterization.

Optics EXPRESS

4. Results and discussion

4.1. Different pitches polishing results

After 60 minutes of continuous polishing, the surface roughness of three different grades of pitch was measured using a white light interferometer. The roughness data at R/2 from the center of the workpiece surface is shown in Fig. 8. The roughness data of the fused silica surface is sampled equidistantly from the center to the edge; six sets of data are measured, and the average value of the six sets of data is collected for each measurement result. It can be seen that among the three polished fused silica glass surfaces, the surface roughness of the No. 55 pitch-processed fused silica glass is the smallest, which is reduced from the initial RMS value of 0.156 nm to 0.114 nm. The No. 73 pitch has the worst result after processing, increasing from the initial RMS value of 0.139 nm to 0.181 nm. The processed low-spatial-frequency part of pitches No. 64 and No. 73 increases significantly.

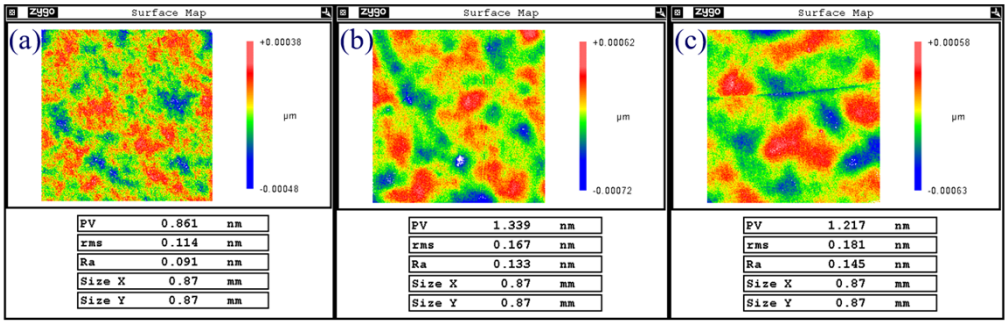

Fig. 8. Surface roughness of fused silica polishing for 60 minutes. (a) Surface roughness of No. 55 pitch after polishing; (b) Surface roughness of No. 64 pitch after polishing; (c) Surface roughness of No. 73 pitch after polishing.

In order to observe the spatial spatial-frequency processing effect of three different types of polished pitches on fused silica glass, the initial surface of fused silica and the central point of the fused silica after processing with the three kinds of pitches, the sampling point data at 20 mm and 40 mm from the center point are drawn on the PSD map, as shown in Fig. 9. Figure 9(a) shows the PSD curve at the center of the workpiece surface before three types of pitches are processed. It is not difficult to see that the PSD curve shapes of the initial surfaces of the three optical elements are very close. Comparing the PSD curves of Fig. 9(b)(c)(d), the low-spatial-frequency part (10^0-10^1/mm) of the fused silica surface after No. 55 pitch polishing is better than the results of the other two kinds of pitch processing and also better than the initial surface. The PSD value of the low-spatial-frequency part is even lower than 10^3nm^3, while No. 64 and No. 73 are poor and close. On the whole, the PSD curves of the surface (10^1-10^3/mm) spatial-frequency band of the three kinds of pitch after polishing have decreased, and the curves are very close. It is known that the smoothing ability of the three kinds of pitch in the middle and high spatial-frequency bands is similar. However, the smoothing ability of pitch No. 55 in the low spatial-frequency part is better than that of the other two pitches.

It can be seen from the above analysis results that the three types of pitch have certain correction capabilities for the10^1-10^3spatial frequency band under the given processing conditions. Compared to the other two brands of pitch, the No. 55 pitch can not only reduce the value of the 10^1-10^3 spatial frequency band but also decrease the value of the 10^0-10^1 spatial frequency band. The plasticity index of No. 64 and No. 73 pitches is much smaller than that of No. 55 pitch. Therefore, it can be seen that polished pitch with a high plasticity index has a greater ability to correct the spatial frequency of the roughness on the surface of optical components.

Optics EXPRESS

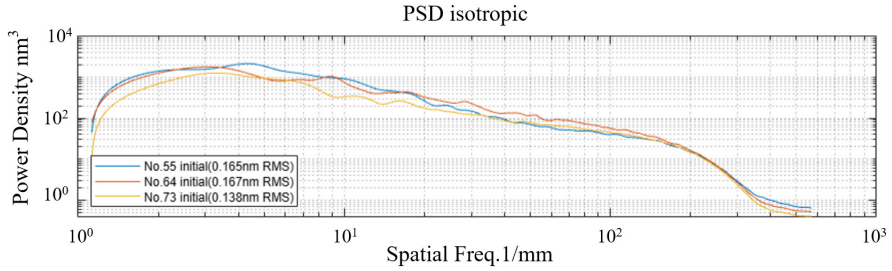

(a)

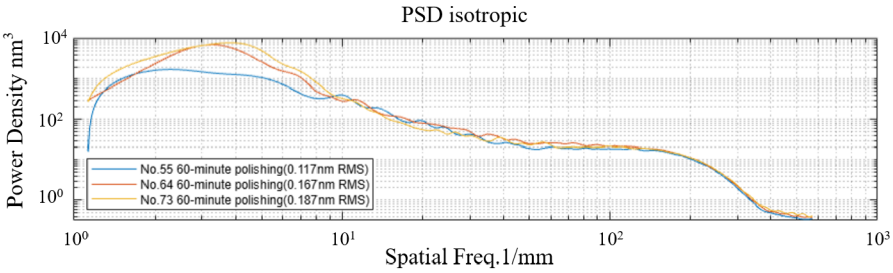

(b)

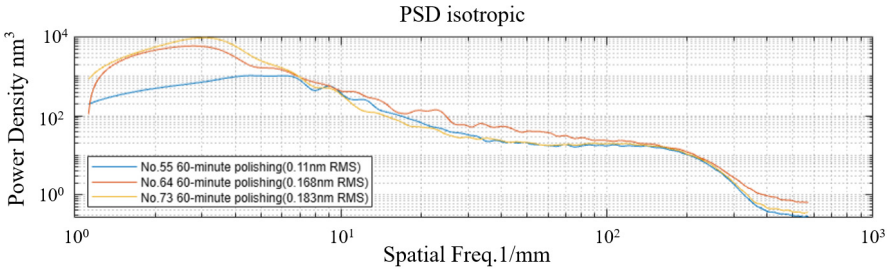

(c)

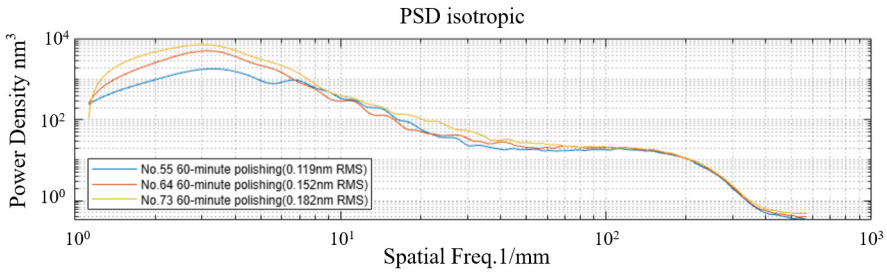

(d)

Fig. 9. PSD curves of different sampling points of three kinds of pitch. (a) PSD curves at the center of the mirror before polishing with three types of pitch; (b) PSD curves at the center of the mirror after polishing with three types of pitch; (c) PSD curves at a distance of 20 mm from the center of the mirror after polishing with three types of pitch; (d) Three PSD curve at 40 mm from the center of the mirror after polishing with three types of pitch.

Optics EXPRESS

4.2. Performance analysis of pitches

The surface morphology of the three types of pitch before and after processing are shown in Fig. 10. After processing No. 55 pitch, the grooves become shallower, the surface deformation is obvious, and pits appear. The processed surface of the No. 64 pitch produced slight deformation and scratches. The surface of the No. 73 pitch shows no obvious deformation and slight scratches after processing. Due to the varying plasticity indices of the three pitches, their macroscopic morphologies differ after polishing. No. 55 pitch has a high plasticity index and is soft, which means it will undergo more deformation during processing. On the contrary, the deformation of the No. 64 and No. 73 pitches is minimal.

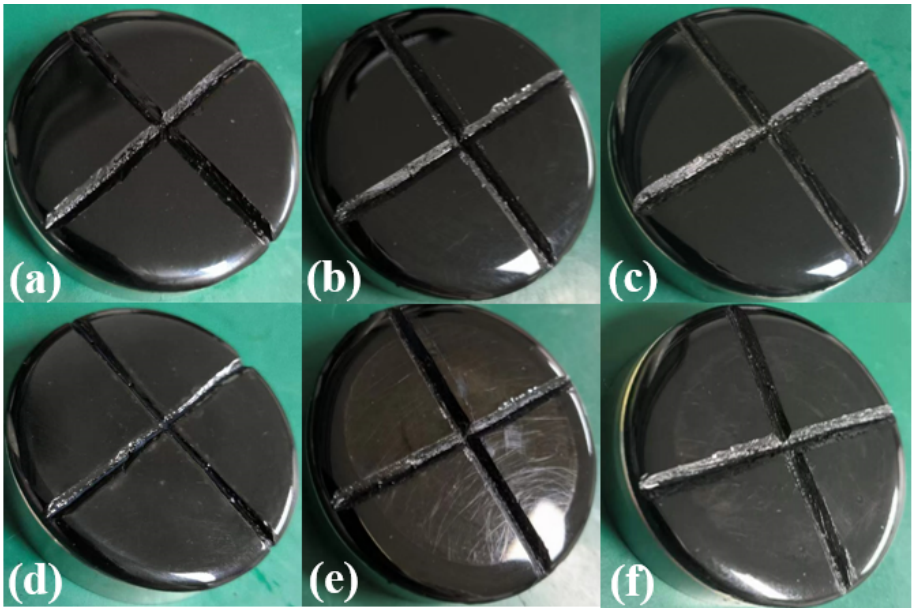

Fig. 10. Changes of surface morphology of three kinds of pitch before and after processing. (a) Before polishing No. 55 pitch; (b) After polishing No. 55 pitch; (c) Before polishing No. 64 pitch; (d) After polishing No. 64 pitch; (e) Before polishing No. 73 pitch; (f) No. 73 pitch After pitch polishing.

Use a laser confocal microscope to observe the surface morphology of three types of pitch after continuous polishing for 60 minutes, and use a 5-times lens to observe the three kinds of pitch surfaces. The results are shown in Fig. 11. The surface of Pitch No. 55 became rough and produced deep pits and scratches, while the surface of Pitch No. 64 developed a large number of scratches and a few shallow pits, and pitch No. 73 had a small number of scratches and pits on its surface, and the surface is smoother than the other two kinds of pitch. This can also explain why the plasticity index of No. 73 is lower than that of No. 55.

4.3. Discussion

Since the properties from the three pitches of Gugolz Company are similar to those of the three types of pitches used in the experiment by Universal Photonics Company [22], the performance parameters in the modeling and analysis process can be used to approximately replace the pitches from Universal Photonics Company. It can be seen from Fig. 3 that the ratio of the elastic-plastic contact area to the actual contact area increases with an increase in the pitch plasticity index. At the same time, it can be seen from the results in Fig. 4 that under the same pressure, the ratio of the actual contact area to the total contact area of the three kinds of pitch is similar.

Optics EXPRESS

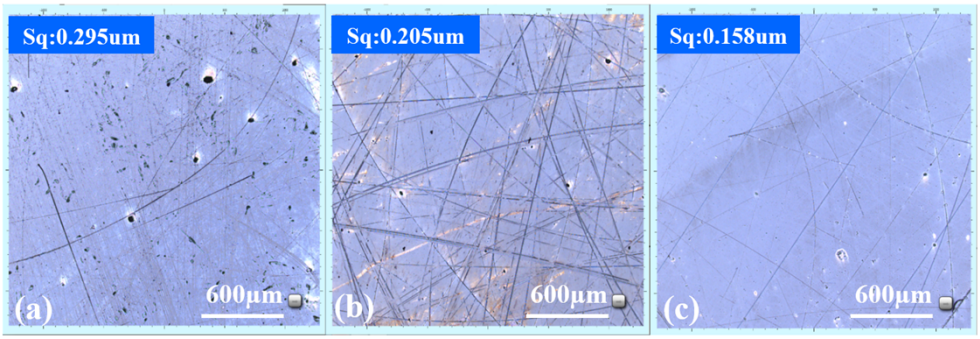

Fig. 11. Morphology of three kinds of pitch after processing. (a) Surface morphology of No. 55 pitch; (b) Surface morphology of No. 64 pitch; (c) Surface morphology of No. 73 pitch.

Therefore, the elastoplastic contact area of the No. 55 pitch is much higher than that of the No. 64 and No. 73 pitch during the actual processing. This can explain why, among the three pitch processing processes, the surface roughness results of the No. 55 pitch and the results of the low-spatial-frequency part of the PSD curve are significantly better than the other two pitches.

As shown in Fig. 12, during the polishing process, elastic-plastic contact mainly occurs due to the high plastic index of No. 55 Pitch. During processing, the pitch surface experiences elastoplastic deformation, which hinders its quick recovery from deformation. As a result, the pitch adheres more easily to the fused silica surface, allowing for better dispersion of polishing abrasive particles in the gap between the two contact planes. During the continuous polishing process, No. 55 pitch facilitates the removal of raised portions on the surface of fused silica. This results in a smoother surface for the fused silica glass and ultimately reduces its roughness value. Additionally, it helps control the low spatial-frequency portion of the PSD curve. For pitches No. 64 and No. 73, the plasticity index is small, indicating that the main deformation is elastic deformation. As a result, the pitch is unable to maintain a stable contact area for an extended period of time. During the polishing process, when the pitch and fused silica come into contact with the upper part of the protrusion, the polishing abrasive grains are unable to fully reach the polishing interface. As a result, a significant amount of abrasive grains accumulate in the pitch gaps, hindering the effective removal of the protrusions. In the end, the surface roughness of the fused silica glass will deteriorate, and the low spatial-frequency portion of the PSD will also deteriorate.

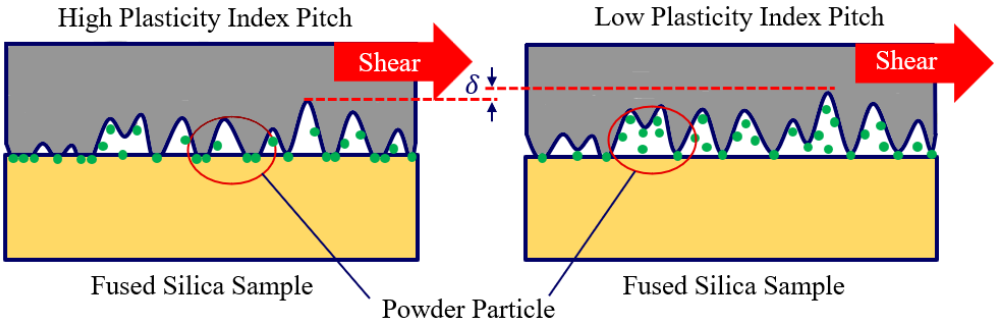

Fig. 12. The contact situation of pitch with different plasticity index and fused silica.

Optics EXPRESS

5. Conclusions

In this paper, we propose an elastoplastic-rough contact model based on the pitch and fused silica glass rough surface, and use the plasticity index to describe the polishing performance of different pitches during the polishing of fused silica glass. At the same time, the plasticity index depends on the material properties of pitch and also depends on its surface morphology. Rough and soft surfaces have a higher plasticity index. After analysis, the ratio of the actual contact area to the total contact area of the three pitches is similar. Under the same polishing pressure, the elastic-plastic contact area of No. 55 pitch and fused silica is much larger than that of No. 64 and No. 73 pitch. The higher the plasticity index, the greater the separation of the pitch contacting the rough surface, resulting in more elastoplastic contact. The results of processing experiments prove that the elastic-plastic contact between pitch and fused silica glass during the polishing process is more conducive to the removal of the raised parts on the surface of fused silica glass, which can improve the surface roughness of fused silica glass to a certain extent and reduce the surface roughness of the medium and high spatial-frequency bands.

The RMS value of the fused silica glass surface, after undergoing No. 55 pitch processing for 60 minutes in a measurement area of $0.87 \times 0.87 \text{mm}^2$ reached 0.114 nm, and the Ra reached 0.091 nm, realizing an atomically flat surface, and the PSD value in the (10^0-10^3/mm) spatial-frequency band was even reduced to below 10^3nm^3. At the same time, this shows that in the process of selecting pitch for engineering experiments in the future, pitch materials with a plasticity index greater than 0.2 can be selected for processing to reduce the roughness of the surface of fused silica glass and finally realize the ultra-smooth surface processing of fused silica. It provides important theoretical guidance for achieving full-diameter, full-band ultra-high precision, and ultra-smooth polishing of large-diameter complex curved surfaces.

Funding. National Natural Science Foundation of China (12203048); Natural Science Foundation of Jilin Province (SKL202302021); National Key Research and Development Program of China (2022YFB3403405).

Disclosures. The authors declare no conflicts of interest.

Data availability. Data underlying the results presented in this paper are not publicly available at this time but may be obtained from the authors upon reasonable request.

References

1. Y. Zhou, H. Luo, and G. Luo, "Chemical mechanical polishing (CMP) of fused silica (FS) using ceria slurry recycling," ECS J. Solid State Sci. Technol. **9**(4), 044002 (2020).
2. F. Kotz, K. Arnold, and W. Bauer, "Three dimensional printing of transparent fused silica glass," Nature **544**(7650), 337–339 (2017).
3. T I. Suratwala, *Materials science and technology of optical fabrication[M]*. John Wiley & Sons, (2018).
4. N. I. Chkhalo, S. A. Churin, and A. E. Pestov, "Roughness measurement and ion-beam polishing of super-smooth optical surfaces of fused quartz and optical ceramics," Opt. Express **22**(17), 20094–20106 (2014).
5. H. Yang, H. Cheng, and Y. Feng, "Improvement of high-power laser performance for super-smooth optical surfaces using elec-trorheological finishing technology," Appl. Opt. **56**(35), 9822–9829 (2017).
6. J. Huang, H. Liu, and F. Wang, "Influence of bulk defects on bulk damage performance of fused silica optics at 355 nm nanosecond pulse laser," Opt. Express **25**(26), 33416 (2017).
7. Z. C. Geng, S. Gao, and R. K. Kang, "Surface layer damage of quartz glass induced by ultra-precision grinding with different grit size," Appl. Mech. Mater. **872**, 19–24 (2017).
8. C. Jiang, T. Wu, and H. Ye, "Estimation of energy and time savings in optical glass manufacturing when using ultrasonic vibration-assisted grinding," Int. J. of Precis. Eng. and Manuf.-Green Tech. **6**(1), 1–9 (2019).
9. H T Liu, Y J, Wan, and Z G Zeng, "Freeform surface grinding and polishing by CCOS based on industrial robot," in *8th International Symposium on Advanced Optical Manufacturing and Testing Technologies: Advanced Optical Manufacturing Technologies* (SPIE 2016), pp.587–593.
10. A. Greenwood J and B. P. Williamson J, "Contact of nominally flat surfaces," Proc. R. Soc. Lond. A **295**(1442), 300–319 (1966).
11. I. McCool J, "Comparison of models for the contact of rough surfaces," Wear **107**(1), 37–60 (1986).
12. W. Akbar and Ö. Ertunç, "A coupled material removal model for chemical mechanical polishing processes," ECS J. Solid State Sci. Technol. **10**(10), 104003 (2021).
13. J. Xia, J. Yu, and S. Lu, "Surface Morphology Evolution during Chemical Mechanical Polishing Based on Microscale Material Removal Modeling for Monocrystalline Silicon," Materials **15**(16), 5641 (2022).

Optics EXPRESS

14. L. Y. Li, C. Y. Wu, and C. Thornton, "A theoretical model for the contact of elastoplastic bodies," Proc. Inst. Mech. Eng., Part C **216**(4), 421–431 (2001).
15. J. Abbott E and A. Firestone F, "Specifying surface quality: a method based on accurate measurement and comparison," J. Mech. Eng. **107**(63), 233–245 (1933).
16. Y. Zhao, M. Maietta D, and L. Chang, "An asperity microcontact model incorporating the transition from elastic deformation to fully plastic flow," J. Trib. **122**(1), 86–93 (2000).
17. S. Oh and J. Seok, "An integrated material removal model for silicon dioxide layers in chemical mechanical polishing processes," Wear **266**(7-8), 839–849 (2009).
18. R. Chang W, I. Etsion, and B. Bogy D, "An elastic-plastic model for the contact of rough surfaces," J. Trib. **109**(2), 257–263 (1987).
19. E Gillman B and F Tinker, "Fun facts about pitch and the pitfalls of ignorance," in *Optical manufacturing and testing* (SPIE 1999), pp.72–79.
20. D. Feit M, P. DesJardin R, and A. Steele W, "Optimized pitch button blocking for polishing high-aspect-ratio optics," Appl. Opt. **51**(35), 8350–8359 (2012).
21. E DeGroote J, D, Jacobs S, and L Gregg, "A data base for the physical properties of optical polishing pitch," in *Optical Fabrication and Testing* (SPIE 2002), p. OTuB2.
22. Q. He, H. Zhang, and J. Li, "Performance evaluation of polyurethane/epoxy resin modified pitch as adhesive layer material for steel-UHPC composite bridge deck pavements," Constr. Build. Mater. **291**, 123364 (2021).

134.102.50.188 {ts '2024-04-12 08:10:47'}